

# Improved description of metal oxide stability

## Beyond the random phase approximation with renormalized kernels

**Jauho, Thomas Stenbæk; Olsen, Thomas; Bligaard, Thomas ; Thygesen, Kristian Sommer**

*Published in:*
Physical Review B

*Link to article, DOI:*
10.1103/physrevb.92.115140

*Publication date:*
2015

*Document Version*
Publisher's PDF, also known as Version of record

# Improved description of metal oxide stability: Beyond the random phase approximation with renormalized kernels

Thomas S. Jauho,[1] Thomas Olsen,[1,2,*] Thomas Bligaard,[3,4] and Kristian S. Thygesen[1,5,†]

[1]*Center for Atomic-Scale Materials Design, Department of Physics, Technical University of Denmark, DK-2800 Kongens Lyngby, Denmark*

[2]*Centro de Física de Materiales, Universidad del País Vasco, 20018 San Sebastían, Spain*

[3]*SUNCAT Center for Interface Science and Catalysis, SLAC National Accelerator Laboratory, 2575 Sand Hill Road, Menlo Park, California 94025, USA*

[4]*Department of Chemical Engineering, Stanford University, Stanford, California 94305, USA*

[5]*Center for Nanostructured Graphene (CNG), Department of Physics, Technical University of Denmark, DK-2800 Kongens Lyngby, Denmark*

(Received 14 July 2015; published 21 September 2015)

The renormalized adiabatic PBE (rAPBE) method has recently been shown to comprise a significant improvement over the random phase approximation (RPA) for total energy calculations of simple solids and molecules. Here we consider the formation energies of 19 group I and II metal oxides and a few transition-metal oxides. The mean absolute error relative to experiments is 0.21 eV and 0.38 eV per oxygen atom for rAPBE and RPA, respectively, and thus the rAPBE method greatly improves the description of metal-oxygen bonds across a wide range of oxides. The failure of the RPA can be partly attributed to the lack of error cancellation between the correlation energy of the oxide on the one hand and the bulk metal and oxygen molecule on the other hand, which are all separately predicted much too negative by the RPA. We ascribe the improved performance of the rAPBE to its significantly better description of absolute correlation energies which reduces the need for error cancellation. The rAPBE is just one out of an entire class of renormalized exchange-correlation kernels which should be further investigated.

DOI: 10.1103/PhysRevB.92.115140 PACS number(s): 71.15.Nc, 71.15.Mb

## I. INTRODUCTION

Metal oxides constitute an important class of inorganic materials that find use in a variety of established and emergent technologies including transparent electrodes, superconductors, microelectronics, batteries, catalysis, photovoltaics, piezoelectrics, and much more. This makes the oxides a very interesting and topical class of materials and drives the need for developing more accurate methods for prediction of their properties. Despite the significant advances made within density functional theory (DFT) it remains a great challenge to compute the ground state energy of metal oxides and their surfaces with the accuracy required for quantitative and predictive modeling. The standard semilocal approximations (LDA/GGA) as well as the (range separated) hybrids suffer from self-interaction and delocalization errors and rely on error cancellation between the exchange and correlation terms. The degree of error cancellation is not complete and for some materials, in particular the oxides, large systematic errors occur [1]. The LDA+$U$ method has been widely used to describe transition-metal oxides with strongly localized $d$ electrons. However, as the results are highly sensitive to $U$, which is typically not calculated *ab initio* but fitted to experiments, the LDA+$U$ method does not qualify as a predictive theory. Moreover, all of these methods fail to account for dispersive interactions. In order to achieve better accuracy it is necessary to go beyond these "standard" DFT approaches.

Quantum chemical methods such as Møller-Plesset perturbation theory or coupled cluster methods are widely used for molecular systems. Recently, both second-order Møller-Plesset theory [2] and coupled cluster [3] have been applied to solids. However, in both cases applications are limited to small systems as the computational cost scales at least as $N^5$, with $N$ being the number of electrons in the system. Recently a full configuration interaction method was applied to solids with promising results, but again at a very high computational cost [4].

Alternatively, one can try to improve the quality of approximations for xc functionals within DFT. One approach is to use the so-called adiabatic connection and fluctuation dissipation theorem (ACFDT) to express the correlation energy in terms of the interacting density-density response function. The correlation energy obtained from the ACFDT must be combined with the exact exchange (EXX) energy and this removes the issue of error cancellation between the two terms as exchange is treated exactly. The simplest version of the ACFDT is the random phase approximation (RPA), where the irreducible response function is simply taken as the noninteracting Kohn-Sham response function. With this approach, Furche assessed the performance of the RPA for atomization energies of a set of small molecules and found an accuracy similar to PBE [5]. Subsequently, the performance of RPA was assessed for bulk properties [6–8] and was shown to yield slightly worse cohesive energies but more accurate lattice constants than the PBE. In addition to its rather accurate account of structural properties, the main merit of the RPA is its accurate description of nonlocal dispersive forces, such as van der Waals interactions. For example, it accurately reproduces the interlayer spacing of graphite [9,10] as well as the binding distance of graphene to various metal surfaces [11,12]. Furthermore, RPA has been shown to give a good account of surface and adsorption energies [13].

While RPA describes long-range interactions much better than semilocal functionals such as PBE, the accuracy of RPA for molecular atomization energies is comparable to or

*tolsen@fysik.dtu.dk

†thygesen@fysik.dtu.dk

 

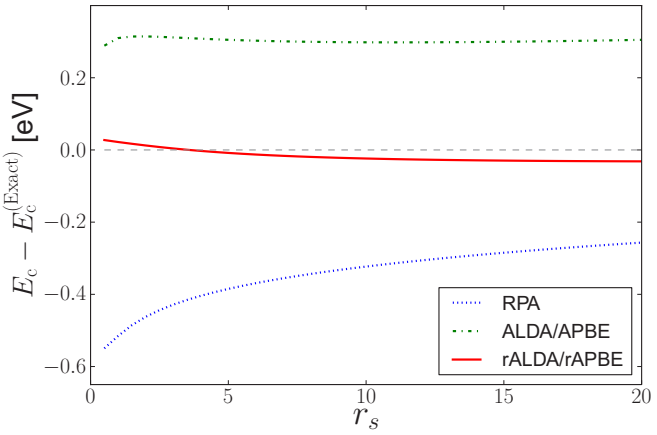


FIG. 1. (Color online) Correlation energy per electron of the homogeneous electron gas calculated with the RPA, ALDA/APBE, and rALDA/rAPBE methods. Note that the (r)ALDA and (r)APBE are identical for the HEG.

worse than PBE [5,10,14,15]. Additionally, total correlation energies are severely underestimated in RPA and reliable results crucially depend on detailed error cancellation between the systems being compared [16]. As exemplified for the homogeneous electron gas (HEG) in Fig. 1, the RPA correlation energy per electron is roughly 0.3–0.5 eV lower than the exact result.

Several attempts have been made to improve on the RPA, such as RPA+ [17], where a GGA short-range correction is introduced, or SOSEX [18], where a second-order screened exchange term is included in order to exactly cancel the one-electron self-correlation error. However, neither of these approaches have led to overall improvements as they perform better for some systems and worse for others [15]. Another promising approach involves the inclusion of electron-hole interactions in the irreducible response function, but this rapidly becomes very computationally demanding [19].

In Refs. [20,21] we showed that the renormalized adiabatic LDA (rALDA) and PBE (rAPBE) kernels provide in general a vast improvement over the RPA. In particular, rALDA/rAPBE greatly improve the description of the absolute correlation energy; see Fig. 1. In Ref. [22] it was shown that the rALDA yields excellent structural properties of solids that are very similar to those obtained from more advanced xc kernels derived from the HEG. Recently, we showed that the rAPBE kernel outperforms both rALDA and RPA for cohesive energies of solids and atomization energies of small molecules [21].

Based on the previous success of the renormalized kernels, the present study sets out to benchmark the performance of the rAPBE for metal oxides in comparison with PBE, BEEF-vdW (a semiempirical optimized Bayesian error estimation functional with van der Waals correlation [23]), and the RPA.

## II. METHOD

### A. The rAPBE

Within the renormalized adiabatic PBE (rAPBE) scheme, the xc energy is calculated non-self-consistently as the sum of the exact exchange (EXX) and the rAPBE correlation energy evaluated on self-consistently determined PBE [24] orbitals and eigenvalues. In practice the total energy is computed as

$$E^{\mathrm{EXX}} = E_{\mathrm{tot}}^{\mathrm{PBE}} - E_{\mathrm{xc}}^{\mathrm{PBE}} + E_{\mathrm{x}}^{\mathrm{EXX}}, \tag{1}$$

$$E^{\mathrm{EXX+rAPBE}} = E^{\mathrm{EXX}} + E_{\mathrm{c}}^{\mathrm{rAPBE}}. \tag{2}$$

Here $E_{\mathrm{tot}}^{\mathrm{PBE}}$ is the self-consistent PBE total energy, $E_{\mathrm{xc}}^{\mathrm{PBE}}$ is the PBE xc energy, $E_{\mathrm{x}}^{\mathrm{EXX}}$ is the exact exchange energy, and $E_{\mathrm{c}}^{\mathrm{rAPBE}}$ is the rAPBE correlation energy obtained from the ACFDT as described below. Note that the term $E^{\mathrm{EXX}}$ is the Hartree-Fock total energy evaluated on PBE orbitals.

The ACFDT expresses the correlation energy in terms of the coupling-constant-dependent response function,

$$E_{\mathrm{c}}[n] = -\int_0^1 d\lambda \int_0^\infty \frac{d\omega}{2\pi} \mathrm{Tr}[v\chi^\lambda(i\omega) - v\chi^{\mathrm{KS}}(i\omega)]. \tag{3}$$

The Kohn-Sham (KS) response function $\chi^{\mathrm{KS}}$ is the exact response function of the noninteracting KS Hamiltonian, while $\chi^\lambda$ gives the response of a system where the electronic interaction, $v = 1/|\mathbf{r} - \mathbf{r}'|$, is scaled by $\lambda$, i.e., $v \to \lambda v$, and the external potential has been chosen such as to produce the ground state density of the fully interacting system.

It is a complicated challenge to calculate the response function of an interacting electron system. However, the linear response formulation of time-dependent DFT (TDDFT) [25] provides an elegant way to express the response function in terms of the Hartree-exchange-correlation (Hxc) kernel through the Dyson equation,

$$\chi^\lambda(\omega) = \chi^{\mathrm{KS}}(\omega) + \chi^{\mathrm{KS}}(\omega) f_{\mathrm{Hxc}}^\lambda(\omega) \chi^\lambda(\omega), \tag{4}$$

where $f_{\mathrm{Hxc}}^\lambda = \lambda v + f_{\mathrm{xc}}^\lambda$ is the Hartree-exchange-correlation kernel. Setting the exchange-correlation kernel, $f_{\mathrm{xc}}^\lambda$, to zero yields the well-known RPA with the response function, $\chi^{\lambda,\mathrm{RPA}} = (1 - \lambda v \chi^{\mathrm{KS}})^{-1} \chi^{\mathrm{KS}}$.

In order to improve on the RPA and correct its consistent underestimation of the correlation energy, a natural step forward is to include the exchange-correlation kernel in the evaluation of $\chi^\lambda$. Reference [21] demonstrated a method for constructing a renormalized adiabatic exchange-correlation kernel using any local or semilocal kernel, rA$X$, such as rALDA or rAPBE. Using this approach, the kernel is given by

$$f_{\mathrm{xc}}^{\mathrm{rA}X}[n](r) = \frac{f_{\mathrm{xc}}^{A X}[n]}{2\pi^2 r^3} \{\sin(q_c[n]r) - q_c[n]r\cos(q_c[n]r)\} - \frac{1}{r}\left[1 - \frac{2}{\pi}\int_0^{q_c[n]r} \frac{\sin x}{x} dx\right], \tag{5}$$

where $q_c[n]$ is a cutoff wave vector introduced in order to remove the unphysical divergence of the on-top correlation hole characteristic of any local xc kernel, while preserving the continuity of $f_{\mathrm{xc}}^{\mathrm{rA}X}(q)$,

$$q_c[n] = \sqrt{\frac{-4\pi}{f_{\mathrm{x}}^{A X}[n]}}, \quad f_{\mathrm{x}}^{A X}[n] < 0. \tag{6}$$

We refer the reader to Ref. [21] for more details on the construction and properties of the renormalized kernels. The rALDA and rAPBE kernels have been implemented in the GPAW electronic structure code [26,27].

### B. The oxides

In this work we consider the formation energy of a set of oxides comprising 19 group I and II oxides and 2 transition-metal oxides. Apart from their general importance, this set of oxides was recently examined using the RPA [28] and experimental formation enthalpies are available making it an ideal case for benchmarking of the renormalized kernels.

The formation energy per oxygen atom was obtained from the computed total energies as

$$\Delta E_{\mathrm{O}} = \frac{1}{y}E[\mathrm{M}_x\mathrm{O}_y] - \frac{x}{y}E[\mathrm{M}] - \frac{1}{2}E[\mathrm{O}_2], \qquad (7)$$

where $E[\mathrm{M}_x\mathrm{O}_y]$, $E[\mathrm{M}]$, and $E[\mathrm{O}_2]$ are the total energies of the oxide, the bulk metal, and the $O_2$ molecule in gas phase.

The lattice constants of the bulk metals and oxides were determined by PBE structure optimizations. The PBE was found to provide the best description of the lattice constants among seven different xc functionals, namely LDA, PBE, RPBE, revPBE, PBEsol, optPBE-vdW, and BEEF-vdW. More specifically, for each of the xc functionals the total energy was calculated as a function of unit cell volume for Li, $Li_2O$, $Li_2O_2$, Na, $Na_2O$, $Na_2O_2$, Ca, and CaO, and the equilibrium volume was found from an equation-of-state fit. Compared to experimental volumes [29] the revPBE and PBE functionals performed the best with mean absolute percentage errors (MAPE) of 5.04% and 5.44%, respectively. Given the small difference in performance between the revPBE and PBE functionals, we chose the PBE for optimizing the lattice constants of all the structures as this constitutes the most consistent choice for the subsequent rAPBE calculations which are based on PBE orbitals and energies as input. Thus both the crystal structures as well as input orbitals for the EXX, RPA, and rAPBE calculations were obtained from the PBE.

The PBE structure optimizations were performed using a 900 eV plane wave cutoff. The Brillouin zone samplings are listed in Table I under $k^{\mathrm{RPA}}$ and correspond to $k$-point densities of $n_k = 4.0$ per $\text{Å}^{-1}$ for oxides and $n_k = 6.0$ per $\text{Å}^{-1}$ for metals. Using PBE to calculate the volumes of all the metals and oxides, the MAPE compared to experimental volumes is 3.71%, with $Li_2O$ and $Cs_2O$ showing the largest deviations of respectively 16.34% and 16.42%. These results are in agreement with the findings of Ref. [28].

TABLE I. Summary of key computational parameters used for the PBE, RPA, and rAPBE calculations. The MP-ID denotes the Material Projects ID from Ref. [29]. For each of the elements, Electrons denotes the number of electrons and, in parenthesis, which states are included in the PAW setup. Spin denotes whether the calculation is spin-polarized (True/False), $k^{\mathrm{EXX}}$ denotes number of $k$ points used for the PBE and EXX calculations, while $E_{\mathrm{cut}}^{\mathrm{RPA}}$ and $k^{\mathrm{RPA}}$ denote the plane wave cutoff range and $k$-point grid used for the RPA and rAPBE calculations.

| | MP-ID | Electrons | Spin | $k^{\mathrm{EXX}}$ | $E_{\mathrm{cut}}^{\mathrm{RPA}}$ | $k^{\mathrm{RPA}}$ |
|---|---|---|---|---|---|---|
| Li | 135 | 1 ($2s$) | F | 16 | 150–400 | 10 |
| $Li_2O$ | 553090 | | F | 16 | 250–400 | 9 |
| $Li_2O_2$ | 841 | | F | 14 | 250–400 | (9,9,3) |
| Na | 127 | 1($3s$) | F | 16 | 150–400 | 13 |
| $Na_2O$ | 2352 | | F | 14 | 250–400 | 8 |
| $Na_2O_2$ | 2340 | | F | 14 | 250–400 | (5,5,6) |
| K | 58 | 9 ($3s3p4s$) | F | 16 | 250–350 | 10 |
| $K_2O$ | 971 | | F | 14 | 280–380 | 7 |
| $K_2O_2$ | 28206 | | F | 14 | 280–380 | (5,5,4) |
| $KO_2$ | 1866 | | T | 14 | 250–350 | 7 |
| Rb | 70 | 9 ($4s4p5s$) | F | 16 | 280–380 | 9 |
| $Rb_2O$ | 1394 | | F | 14 | 280–380 | 6 |
| $Rb_2O_2$ | 7895 | | F | 14 | 280–380 | (7,5,5) |
| $RbO_2$ | 12105 | | T | 14 | 280–380 | 7 |
| Cs | 1 | 9 ($5s5p6s$) | F | 16 | 280–380 | 9 |
| $Cs_2O$ | 7988 | | F | 14 | 280–380 | 7 |
| $Cs_2O_2$ | 7896 | | F | 14 | 280–350 | (7,5,5) |
| $CsO_2$ | 1441 | | T | 14 | 280–380 | 7 |
| Be | 87 | 2 ($2s$) | F | 16 | 250–350 | (19,19,11) |
| BeO | 2542 | | F | 14 | 280–380 | (11,11,6) |
| Mg | 153 | 10 ($2s2p3s$) | F | 16 | 250–400 | (14,14,7) |
| MgO | 1265 | | F | 16 | 280–400 | 10 |
| Ca | 132 | 10 ($3s3p4s$) | F | 16 | 250–350 | (11,11,6) |
| CaO | 2605 | | F | 16 | 280–380 | 9 |
| $CaO_2$ | 634859 | | F | 14 | 280–380 | 8 |
| Sr | 19999 | 10 ($4s4p5s$) | F | 16 | 250–350 | 11 |
| SrO | 2472 | | F | 14 | 280–380 | 8 |
| Ba | 122 | 10 ($5s5p6s$) | F | 16 | 250–350 | 10 |
| BaO | 1342 | | F | 14 | 280–380 | 8 |
| Ti | 72 | 12($3s3p3d4s$) | F | 20 | 250–400 | (6,6,9) |
| $TiO_2$ | 2657 | | F | 14 | 280–380 | (5,5,9) |
| Ru | 33 | 16($4s4p4d5s$) | F | 16 | 280–380 | (11,11,6) |
| $RuO_2$ | 9449 | | F | 16 | 280–380 | (8,6,6) |

### C. Computational details

The PBE and EXX calculations were performed using very high Brillouin zone samplings of $16 \times 16 \times 16$ and $14 \times 14 \times 14$ in general for the metals and the oxides, respectively. A plane wave (PW) basis set with 900 eV cutoff energy was used for all PBE and EXX calculations. BEEF-vdW total energies were calculated for the PBE relaxed structures, using the same $k$-point samplings as used for PBE and EXX, and a PW cutoff of 600 eV for the metals and 900 eV for the oxides. The exchange energy entering the RPA and rAPBE total energies was computed using the Wigner-Seitz truncation of the Coulomb interaction which was recently shown to provide better convergence with respect to $k$-point sampling [30]. The PBE, BEEF-vdW, and EXX calculations for the oxygen molecule used a PW cutoff of 900 eV and a unit cell defined by a vacuum distance of 10 Å between neighboring molecules. We used PAW potentials with semicore states included for most elements. Table I shows the number of electrons included in the PAW calculations for each of the metals and oxides.

For the rAPBE and RPA correlation energy calculations we used the same Brillouin zone samplings as used for the structure optimizations, i.e., $k$-point density set to $n_k = 4.0$ per $\text{Å}^{-1}$ for oxides and $n_k = 6.0$ per $\text{Å}^{-1}$ for metals. The specific $k$-point grids used for each system are listed in Table I. The number of unoccupied bands included in the calculations was set equal to the number of plane waves.

The rAPBE/RPA calculations converge very slowly with the number of unoccupied bands included in the noninteracting response function. Reference [6] showed that in

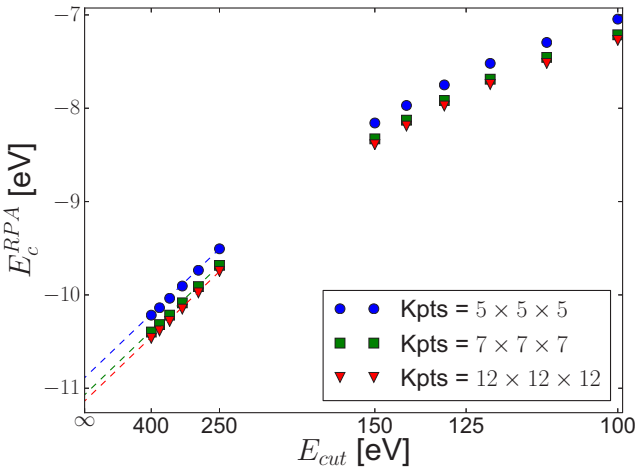


FIG. 2. (Color online) The RPA correlation energy of Mg as function of the plane wave cutoff for different $k$-point samplings. The difference between the curves is essentially constant implying that the $k$-point convergence and extrapolation to infinite plane wave cutoff can be treated separately. The number of empty bands included in $\chi_0$ is always set equal to the number of plane waves.

the high-energy limit, the correlation energy converges as $E_c^{\text{Lindhard}}(E_{\text{cut}}) = E_c^{\infty} + A/E_{\text{cut}}^{3/2}$ for RPA calculations. We have found empirically that the same scaling applies to the rAPBE. To obtain the converged RPA and rAPBE correlation energies we extrapolated six uniformly spaced cutoff energies in the energy ranges given under $E_{\text{cut}}^{\text{rAPBE}}$ in Table I, in order to obtain $E_c^{\text{rAPBE}}$ and $E_c^{\text{RPA}}$.

It is possible to greatly reduce the computational costs by converging $k$ points and PW cutoff (and thus number of empty bands in $\chi_0$) separately. This is possible because the difference in correlation energy obtained with two different $k$-point samplings is nearly independent of the PW cutoff. Consequently, we perform the extrapolation to infinite PW cutoff using a coarser $k$-point grid, and the difference between the correlation energy evaluated at 150 eV cutoff using the coarse and converged $k$-point grids. Figure 2 demonstrates how the energy difference at $E_{\text{cut}} = 150$ eV is added to the energies in the range 250 eV to 400 eV.

The $k$-point grids used for the RPA and rAPBE calculations are similar or higher than those used in Ref. [28], which reported convergence within 50 meV for RPA oxide formation energies. References [21,22] showed that rAPBE converges as fast or faster than RPA with respect to $k$ points.

The RPA and rAPBE correlation energies for $O_2$ were performed spin-polarized (with a magnetic moment of 2 $\mu_B$) using 5 Å vacuum between periodically repeated molecules, and the correlation energy was extrapolated based on four computed points with plane wave cutoff in the interval 345–420 eV. The RPA was found to be converged to within 20 meV with respect to the unit cell size.

We mention that zero-point energy (ZPE) contributions were not included in calculating formation energies from Eq. (7). Reference [28] examined the effect of including ZPEs calculated within the harmonic approximation with PBE and found that the MAE of the formation energy changed by less than 0.01 eV.

TABLE II. Calculated and experimental oxide formation energies per oxygen atom. For each method the mean error (ME) in eV, the mean absolute error (MAE) in eV, and the mean absolute percentage error (MAPE) are given. All experimental values are taken at room temperature.

| | PBE | BEEF-vdW | EXX | RPA | rAPBE | Expt. |
|---|---|---|---|---|---|---|
| $Li_2O$ | −5.41 | −5.67 | −5.83 | −5.71 | −5.95 | −6.14 |
| $Li_2O_2$ | −2.77 | −2.91 | −2.59 | −2.91 | −3.10 | −3.28 |
| $Na_2O$ | −3.56 | −3.81 | −3.37 | −3.83 | −4.07 | −4.28 |
| $Na_2O_2$ | −2.10 | −2.25 | −1.87 | −1.99 | −2.30 | −2.63 |
| $K_2O$ | −3.03 | −3.24 | −2.17 | −3.16 | −3.24 | −3.76 |
| $K_2O_2$ | −2.09 | −2.23 | −1.57 | −1.96 | −2.11 | −2.57 |
| $KO_2$ | −1.30 | −1.33 | 0.12 | −1.21 | −1.51 | −1.48 |
| $Rb_2O$ | −2.66 | −2.87 | −1.54 | −2.95 | −3.10 | −3.51 |
| $Rb_2O_2$ | −1.96 | −2.09 | −1.33 | −2.10 | −2.26 | −2.48 |
| $RbO_2$ | −1.28 | −1.28 | 0.20 | −1.25 | −1.50 | −1.45 |
| $Cs_2O$ | −3.00 | −3.43 | −1.22 | −3.05 | −2.88 | −3.58 |
| $Cs_2O_2$ | −1.98 | −2.10 | −1.19 | −2.09 | −2.25 | −2.58 |
| $CsO_2$ | −1.31 | −1.33 | 0.23 | −1.22 | −1.49 | −1.48 |
| BeO | −5.39 | −5.47 | −6.27 | −5.94 | −6.13 | −6.27 |
| MgO | −5.37 | −5.43 | −6.02 | −5.99 | −6.17 | −6.19 |
| CaO | −5.85 | −6.06 | −6.01 | −6.09 | −6.41 | −6.55 |
| $CaO_2$ | −2.80 | −2.94 | −2.59 | −3.02 | −3.36 | −3.17 |
| SrO | −5.41 | −5.65 | −5.44 | −5.78 | −6.00 | −6.11 |
| BaO | −4.97 | −5.23 | −5.08 | −5.51 | −5.61 | −5.67 |
| $TiO_2$ | −4.43 | −4.45 | −5.15 | −4.52 | −4.76 | −4.90 |
| $RuO_2$ | −1.54 | −1.53 | −0.73 | −1.42 | −1.65 | −1.58 |
| ME | −0.55 | −0.40 | −0.96 | −0.38 | −0.18 | |
| MAE | 0.55 | 0.40 | 0.99 | 0.38 | 0.21 | |
| MAPE | 14.66% | 10.85% | 39.35% | 12.09% | 6.57% | |

## III. RESULTS AND DISCUSSION

### A. Formation energies

The formation energies computed with PBE, BEEF-vdW, EXX, RPA, and rAPBE are given in Table II and summarized in Fig. 3. The BEEF-vdW was included here to compare

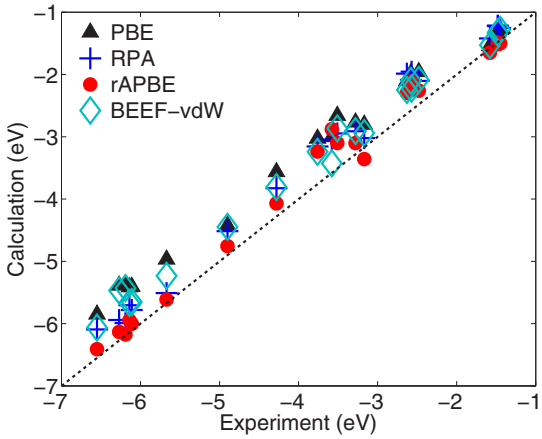


FIG. 3. (Color online) Formation energy per oxygen atom for the oxides listed in Table II. The formation energies calculated using PBE, BEEF-vdW, RPA, and rAPBE are plotted against the experimental values.

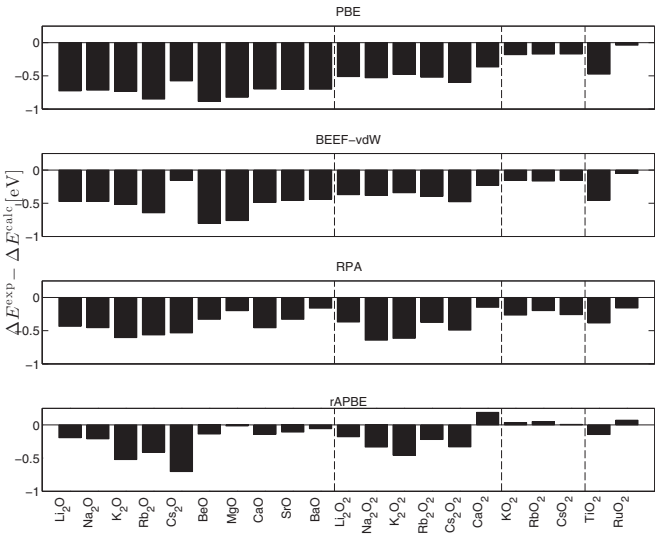


FIG. 4. The differences between the experimental and calculated formation energies obtained with PBE, BEEF-vdW, RPA, and rAPBE. The oxides are ordered from left to right by type: oxides, peroxides, superoxides, and transition-metal oxides.

the performance of the *ab initio* RPA and rAPBE methods to a density functional that includes long-range interactions. The mean error (ME), mean absolute error (MAE), and mean absolute percentage error (MAPE) with respect to experiment are shown in the last three rows of the table. Comparing the ME and MAE shows that the PBE, BEEF-vdW, EXX, and RPA formation energies all have a clear and consistent bias towards too high formation energies; i.e., oxides are predicted less stable than found in experiment (see Ref. [28] for references on the experimental data). While rAPBE shows the same tendency to underbinding, it is less pronounced, and $CaO_2$, $KO_2$, $CsO_2$, and $RuO_2$ are in fact predicted to be more stable than experiment. The rAPBE method outperforms all of the other methods with a MAE of only 0.21 eV compared to 0.38 eV for RPA and 0.40 for BEEF-vdW. This translates into a MAPE of only 6.57 % for rAPBE, while RPA has a MAPE of 13.39 %; see Table II.

For clarity the deviations from experiment ($\Delta E_O^{exp} - \Delta E_O^{calc}$) are plotted separately for each xc functional in Fig. 4. The panels are ordered from top to bottom by increasing complexity of the method and the oxides are ordered from left to right by oxide type: oxides, peroxides, superoxides, and transition-metal oxides. In the top panel PBE performs the worst with a MAE of 0.51 eV. The PBE energies display a clear trend in the error with respect to the oxide type: While the oxides (left) show a large MAE of 0.74 eV, the peroxides (middle) and superoxides (right) have MAEs of 0.50 eV and 0.15 eV, respectively. The same trend is observed for the BEEF-vdW, while the quality of the RPA and rAPBE results are largely independent of the oxide type.

In practice, a consistent systematic error in the formation energies can be corrected by fitting the energy of the oxygen molecule as this introduces a constant shift in the formation energy. This strategy is further motivated by the fact that the total energy of $O_2$ is known to be difficult to calculate accurately, within standard approximations for the xc functional. However, it is well known that RPA severely underestimates the total correlation energies for solids as well as molecules and the error can therefore not be associated with the description of the $O_2$ molecule alone. Nevertheless, there may be systematic trends in the lack of error cancellation for these systems, which justifies a fitting procedure for RPA as well. Thus using the $O_2$ energy as a fitting parameter for removing the bias for each method, the MAE becomes 0.19 eV, 0.15 eV, 0.13 eV, and 0.17 eV for PBE, BEEF-vdW, RPA, and rAPBE, respectively. It is noted that the RPA error is reduced by 0.25 eV while the rAPBE error is only improved by 0.04 eV. This is due to the fact that the superoxides are very well described by rAPBE and fitting the oxygen energy worsens the formation energies of the superoxides compared to experiment.

TABLE III. Correlation energies of the metals, oxides, and $O_2$. The energies are given in eV per electron. The last column indicates the difference between the RPA and rAPBE correlation energy per electron.

| | $E_c^{RPA}$ | $E_c^{rAPBE}$ | $E_c^{rAPBE} - E_c^{RPA}$ |
|---|---|---|---|
| $O_2$ | −1.75 | −1.20 | 0.55 |
| Li | −1.49 | −1.10 | 0.39 |
| Na | −1.29 | −0.94 | 0.35 |
| K | −1.34 | −0.95 | 0.39 |
| Rb | −1.14 | −0.78 | 0.35 |
| Cs | −1.28 | −0.83 | 0.46 |
| Be | −1.63 | −1.18 | 0.45 |
| Mg | −0.56 | −0.43 | 0.13 |
| Ca | −1.34 | −0.99 | 0.35 |
| Sr | −1.19 | −0.86 | 0.33 |
| Ba | −1.44 | −0.98 | 0.46 |
| Ti | −1.68 | −1.39 | 0.30 |
| Ru | −1.33 | −1.11 | 0.22 |
| $Li_2O$ | −1.67 | −1.19 | 0.48 |
| $Li_2O_2$ | −1.76 | −1.26 | 0.50 |
| $Na_2O$ | −1.69 | −1.23 | 0.47 |
| $Na_2O_2$ | −1.70 | −1.23 | 0.48 |
| $K_2O$ | −1.49 | −1.06 | 0.43 |
| $K_2O_2$ | −1.53 | −1.09 | 0.45 |
| $KO_2$ | −1.70 | −1.25 | 0.45 |
| $Rb_2O$ | −1.35 | −0.95 | 0.40 |
| $Rb_2O_2$ | −1.44 | −1.01 | 0.42 |
| $RbO_2$ | −1.63 | −1.19 | 0.44 |
| $Cs_2O$ | −1.48 | −0.99 | 0.49 |
| $Cs_2O_2$ | −1.53 | −1.05 | 0.48 |
| $CsO_2$ | −1.69 | −1.21 | 0.48 |
| BeO | −1.68 | −1.18 | 0.50 |
| MgO | −1.00 | −0.73 | 0.28 |
| CaO | −1.50 | −1.10 | 0.40 |
| $CaO_2$ | −1.60 | −1.18 | 0.43 |
| SrO | −1.42 | −1.02 | 0.40 |
| BaO | −1.58 | −1.10 | 0.49 |
| $TiO_2$ | −1.66 | −1.26 | 0.40 |
| $RuO_2$ | −1.56 | −1.22 | 0.34 |
| MD (metals) | | | 0.35 |
| MD (oxides) | | | 0.44 |

Another study [28] of a very similar set of oxides found, with the same fitting of the $O_2$ energy, MAEs for PBE and RPA of 0.21 eV and 0.10 eV, respectively. While these values are in excellent agreement with our results, we note that Ref. [28] finds somewhat better agreement between experiment and RPA for the bare, i.e., unfitted, formation energies than we find in the present work. In fact, comparing the contribution to the formation energy due to the RPA correlation energy we find a mean absolute difference of 0.14 eV between the present work and Ref. [28]. In comparison our PBE results only differ by 0.07 eV. We ascribe this deviation to the different PW cutoff and $k$-point samplings used for the RPA calculations in the two studies.

### B. Absolute correlation energies

The correlation energies from rAPBE and RPA are given for the bulk metals and oxides in Table III in eV per valence electron. There is a clear systematic trend showing that rAPBE consistently yields less negative correlation energies than RPA. The mean difference (MD) is 0.35 (0.44) eV per electron for metals (oxides). For $O_2$, the correlation energy per electron is 0.55 eV larger with rAPBE than with RPA. As shown in Fig. 1, RPA underestimates the correlation energy per electron for the HEG by 0.3–0.5 eV over the relevant range of densities, while rALDA/rAPBE is within 0.05 eV of the exact correlation energy. Similarly, RPA yields a correlation energy of −0.6 eV for the hydrogen atom while rAPBE is very close to the exact result of zero. Consequently, much of the success of the RPA must be ascribed to a detailed error cancellation. The results obtained in this study suggest that rAPBE greatly improves the description of the correlation energy in not only the HEG but also for metals and metal oxides. This also agrees very well with previous studies, which found significant improvements in correlation energy when compared to RPA and exact values for a range of small molecules [20,21,31].

## IV. CONCLUSION

We have calculated the formation energy of 21 metal oxides using the PBE, BEEF-vdW, EXX, RPA, and rAPBE methods and compared to experimental values. The formation energies obtained with the rAPBE are closest to experiments, with a mean absolute error (MAE) per oxygen of only 0.21 eV. In comparison the MAE obtained with the RPA is 0.38 eV while those of BEEF-vdW and PBE are 0.40 eV and 0.55 eV, respectively. All the methods were found to systematically underestimate the stability of the oxides with the rAPBE showing the least systematic deviations from experiments. As a consequence, the results obtained with the rAPBE improve only marginally when the energy of the $O_2$ molecule is fitted to minimize the deviation from the experimental formation energy while the results obtained with the other methods can be significantly improved by this method. For the correlation energies, rAPBE consistently finds energies of around 0.4 eV/electron higher (less negative) than the RPA, suggesting that rAPBE, to a large extent, corrects the systematic underestimation of the correlation energy by the RPA. These systematic errors in the RPA correlation energies are not accurately canceled when evaluating the formation energies. Thus the improved description of oxide formation energies by the rAPBE can be ascribed to its better description of absolute correlation energies.

## ACKNOWLEDGMENTS

The authors acknowledge support from the Danish Council for Independent Research's Sapere Aude Program, Grant No. 11-1051390. The Center for Nanostructured Graphene is sponsored by the Danish National Research Foundation, Project DNRF58. T.B. thanks DOE-BES for funding to SUNCAT.

[1] L. Wang, T. Maxisch, and G. Ceder, Phys. Rev. B **73**, 195107 (2006).
[2] A. Grüneis, M. Marsman, and G. Kresse, J. Chem. Phys. **133**, 074107 (2010).
[3] B. Paulus, Phys. Rep. **428**, 1 (2006).
[4] G. H. Booth, A. Gruneis, G. Kresse, and A. Alavi, Nature (London) **493**, 365 (2013).
[5] F. Furche, Phys. Rev. B **64**, 195120 (2001).
[6] J. Harl and G. Kresse, Phys. Rev. B **77**, 045136 (2008).
[7] J. Harl and G. Kresse, Phys. Rev. Lett. **103**, 056401 (2009).
[8] J. Harl, L. Schimka, and G. Kresse, Phys. Rev. B **81**, 115126 (2010).
[9] S. Lebègue, J. Harl, T. Gould, J. G. Ángyán, G. Kresse, and J. F. Dobson, Phys. Rev. Lett. **105**, 196401 (2010).
[10] T. Olsen and K. S. Thygesen, Phys. Rev. B **87**, 075111 (2013).
[11] T. Olsen, J. Yan, J. J. Mortensen, and K. S. Thygesen, Phys. Rev. Lett. **107**, 156401 (2011).
[12] F. Mittendorfer, A. Garhofer, J. Redinger, J. Klimes, J. Harl, and G. Kresse, Phys. Rev. B **84**, 201401(R) (2011).
[13] L. Schimka, J. Harl, A. Stroppa, A. Grüneis, M. Marsman, F. Mittendorfer, and G. Kresse, Nat. Mater. **9**, 741 (2010).
[14] H. Eshuis, J. Bates, and F. Furche, Theor. Chem. Acc. **131**, 1084 (2012).
[15] X. Ren, P. Rinke, C. Joas, and M. Scheffler, J. Mater. Sci. **47**, 7447 (2012).
[16] M. Lein, E. K. U. Gross, and J. P. Perdew, Phys. Rev. B **61**, 13431 (2000).
[17] Z. Yan, J. P. Perdew, and S. Kurth, Phys. Rev. B **61**, 16430 (2000).
[18] A. Grüneis, M. Marsman, J. Harl, L. Schimka, and G. Kresse, J. Chem. Phys. **131**, 154115 (2009).
[19] T. Olsen and K. S. Thygesen, J. Chem. Phys. **140**, 164116 (2014).
[20] T. Olsen and K. S. Thygesen, Phys. Rev. B **86**, 081103(R) (2012).
[21] T. Olsen and K. S. Thygesen, Phys. Rev. Lett. **112**, 203001 (2014).
[22] C. E. Patrick and K. S. Thygesen, J. Chem. Phys. **143**, 102802 (2014).
[23] J. Wellendorff, K. T. Lundgaard, A. Møgelhøj, V. Petzold, D. D. Landis, J. K. Nørskov, T. Bligaard, and K. W. Jacobsen, Phys. Rev. B **85**, 235149 (2012).
[24] J. Perdew, K. Burke, and M. Ernzerhof, Phys. Rev. Lett. **77**, 3865 (1996).

[25] E. Runge and E. K. U. Gross, Phys. Rev. Lett. **52**, 997 (1984).
[26] J. Enkovaara, C. Rostgaard, J. J. Mortensen, J. Chen, M. Dulak, L. Ferrighi, J. Gavnholt, C. Glinsvad, V. Haikola, H. A. Hansen, H. H. Kristoffersen, M. Kuisma, A. H. Larsen, L. Lehtovaara, M. Ljungberg, O. Lopez-Acevedo, P. G. Moses, J. Ojanen, T. Olsen, V. Petzold, N. A. Romero, J. Stausholm-Møller, M. Strange, G. A. Tritsaris, M. Vanin, M. Walter, B. Hammer, H. Häkkinen, G. K. H. Madsen, R. M. Nieminen, J. K. Nørskov, M. Puska, T. T. Rantala, J. Schiøtz, K. S. Thygesen, and K. W. Jacobsen, J. Phys.: Condens. Matter **22**, 253202 (2010).
[27] J. Yan, J. J. Mortensen, K. W. Jacobsen, and K. S. Thygesen, Phys. Rev. B **83**, 245122 (2011).
[28] J. Yan, J. S. Hummelshøj, and J. K. Nørskov, Phys. Rev. B **87**, 075207 (2013).
[29] A. Jain, S. P. Ong, G. Hautier, W. Chen, W. D. Richards, S. Dacek, S. Cholia, D. Gunter, D. Skinner, G. Ceder, and K. A. Persson, APL Mater. **1**, 011002 (2013).
[30] R. Sundararaman and T. A. Arias, Phys. Rev. B **87**, 165122 (2013).
[31] T. Olsen and K. S. Thygesen, Phys. Rev. B **88**, 115131 (2013).